

## PARASITE GENETICS

# A single-cell RNA-seq atlas of *Schistosoma mansoni* identifies a key regulator of blood feeding

George Wendt<sup>1\*</sup>, Lu Zhao<sup>1\*</sup>, Rui Chen<sup>1</sup>, Chenxi Liu<sup>2</sup>, Anthony J. O'Donoghue<sup>2</sup>, Conor R. Caffrey<sup>2</sup>, Michael L. Reese<sup>1,3</sup>, James J. Collins III<sup>1†</sup>

Schistosomiasis is a neglected tropical disease that infects 240 million people. With no vaccines and only one drug available, new therapeutic targets are needed. The causative agents, schistosomes, are intravascular flatworm parasites that feed on blood and lay eggs, resulting in pathology. The function of the parasite's various tissues in successful parasitism are poorly understood, hindering identification of therapeutic targets. Using single-cell RNA sequencing (RNA-seq), we characterize 43,642 cells from the adult schistosome and identify 68 distinct cell populations, including specialized stem cells that maintain the parasite's blood-digesting gut. These stem cells express the gene *hnf4*, which is required for gut maintenance, blood feeding, and pathology *in vivo*. Together, these data provide molecular insights into the organ systems of this important pathogen and identify potential therapeutic targets.

**S**chistosomes dwell inside the host's circulation, often for decades, where they feed on blood and lay eggs, which become trapped in host tissues and cause disease pathology. Because this parasite is a metazoan composed of multiple tissue types, understanding the schistosome's biology on a molecular level during parasitism could suggest therapeutic strategies. Single-cell RNA sequencing (scRNA-seq) has been used to comprehensively describe tissue types and physiology of diverse metazoans (1), including larval schistosomes (2), but we lack a comprehensive description of the cell types present in egg-laying adults because specific molecular markers are known for only a small number of cell types (3–8).

To define the molecular signature of adult schistosome cell types, we dissociated adult *Schistosoma mansoni*, isolated cells by fluorescence-activated cell sorting (FACS), and generated scRNA-seq libraries using a 10x genomics chromium controller (fig. S1A). Schistosomes are dioecious, and sexual maturation of the female worm's reproductive organs, including the ovary and vitellaria, requires sustained physical contact with the male worm (9). Accordingly, we generated scRNA-seq libraries from adult male parasites, adult sexually mature female parasites, and age-matched virgin female parasites. We then performed clustering, identifying 68 molecularly distinct clusters composed of 43,642 cells (Fig. 1A, fig. S1B, and table S1). These included three clusters of cells expressing somatic stem cell (i.e., neoblast) markers such as the RNA bind-

ing protein *nanos2*, the cell surface receptor *notch*, and the receptor tyrosine kinase *fgfra* (3) (Fig. 1B and fig. S2A); eight clusters expressing markers of tegument (“skin”-like surface) progenitors (4, 5) (fig. S2B); two clusters of parenchymal cells (Fig. 1C and fig. S2C); one cluster of ciliated flame cells that are part of the worm's protonephridial (excretory) system (Fig. 1D and fig. S2D); eight clusters of muscles (Fig. 1E); and a cluster of esophageal gland cells (Fig. 1F and fig. S2E). Despite being composed of thousands of nuclei, our analysis also identified clusters corresponding to syncytial tissues: the tegument (4) (Fig. 1G and fig. S2F) and gut (Fig. 1H and fig. S2G). We failed to identify cells from the female ootype (an organ involved in eggshell formation) (9) and the protonephridial ducts (10), possibly because of their multinucleate nature. Gene ontology analyses of these clusters (table S2) confirmed expected findings (enrichment of “DNA replication” in “neoblast 1”) and revealed previously uncharacterized biology such as the enrichment of “extracellular matrix structural components” in muscle clusters, suggesting that muscles are the source of extracellular matrix in schistosomes, similar to planarians (11).

We uncovered unexpected molecular complexity within the schistosome nervous system, identifying 30 clusters expressing the neuroendocrine protein *7b2* (Fig. 1I) and one apparent neuronal cluster that did not express high levels of *7b2* but did express several synaptic molecules (e.g., *synapsin*) (fig. S3A and table S1). Examination of genes from these neuronal cell clusters uncovered distinct molecular fingerprints for several populations (figs. S3, A to E, and S4; and table S1) and highly ordered structural and regional specialization in the central and peripheral nervous systems, including left-right asymmetry (fig. S3B) and nine types of apparently ciliated neurons (fig. S3, C and D). This complexity is surprising, given the relatively “sedentary”

lifestyle of adult parasites in the portal vasculature (9).

Schistosome muscle is also very heterogeneous, with eight muscle clusters that possess distinctive expression patterns (fig. S5, A to C). Some populations occur diffusely throughout the animal (muscle 1 and muscle 2), whereas others are anatomically restricted, such as muscle 7 cells that reside next to the gut, suggesting that they are enteric muscles.

Similar to planarians (12), many morphogens that regulate Wnt (fig. S6, A to D) and TGF- $\beta$  signaling (fig. S6, E to H) are expressed in muscle and neuronal cells of schistosomes. Homologs of many of these genes are expressed specifically in planarian muscles (1) and have been implicated in regeneration in planarians (12). Though schistosomes survive amputation (13), there is no evidence of whole-body regeneration. This expression pattern in a nonregenerative animal suggests that these genes may regulate schistosome neoblasts during homeostasis.

The pathology of schistosome infection is driven by the host's inflammatory responses to parasite eggs (14). Thus, we examined the differences between male, sexually mature female, and age-matched virgin females at the cellular level (Fig. 2A). All adult parasites have germline stem cells (GSCs) marked by expression of *nanos1* (6). Our scRNA-seq data revealed that GSCs have very similar gene expression regardless of sex or maturity (Fig. 2B and fig. S7A). Like GSCs, GSC progeny fall into the same clusters in both male and female parasites, suggesting no major sex- or maturation-dependent differences in early gametogenesis (Fig. 2C and fig. S7B). However, later germ cells cluster according to sex, with expression of late female germ cell markers found predominantly in mature females (Fig. 2D and fig. S7C) and late male germ cell markers found only in males (fig. S7D).

The sexually mature schistosome ovary is structured such that GSCs reside at the anterior end and mature oocytes at the posterior end (6, 15). The GSC marker *nanos1* is expressed in the proliferative anterior compartment (Fig. 2B, top, and fig. S8, A to D), whereas the late female germ cell marker *bmpg* is expressed most highly in the posterior ovary (Fig. 2D, top, and fig. S8C). Our scRNA-seq data show that the GSC progeny cluster sits between GSCs and late female germ cells on the uniform manifold approximation and projection (UMAP) plot (Fig. 2A), with the GSC progeny marker *meiob* expressed most highly between the anterior and posterior ovary (Fig. 2C and fig. S7B). Concurrent visualization of these clusters reveals an organized linear architecture (fig. S8E). Notably, both mature and virgin females express the marker *meiob* (Fig. 2C), suggesting that virgin female GSCs express differentiation markers without

<sup>1</sup>Department of Pharmacology, UT Southwestern Medical Center, Dallas, TX 75390, USA. <sup>2</sup>Center for Discovery and Innovation in Parasitic Diseases, Skaggs School of Pharmacy and Pharmaceutical Sciences, University of California, San Diego, 9500 Gilman Dr., La Jolla, CA 92093, USA.

<sup>3</sup>Department of Biochemistry, UT Southwestern Medical Center, Dallas, TX 75390, USA.

\*These authors contributed equally to this work.

†Corresponding author. Email: jamesj.collins@utsouthwestern.edu

male stimulus. Thus, male parasites may regulate this developmental checkpoint by promoting survival of differentiating GSCs rather than by inducing commitment, consistent with studies suggesting that male-female pairing can suppress apoptosis in the vitellaria of virgin female worms (16).

We also examined the vitellaria, another male-sensitive, stem cell-dependent tissue that

produces the yolk cells of the parasite's eggs. Despite a different function and organization, we observed parallels between ovary and vitellaria maturation, such as an apparent lineage from stem cell to mature tissue (fig. S9, A to D). We also found a low frequency of vitellocyte-like cells in males (17) (fig. S9A). Finally, we identified pairing-independent sexual tissues such as the flatworm-specific Mehlis' gland,

which plays an enigmatic role in egg production (9) (fig. S9E).

In addition to sexual tissues, we observed sexual dimorphism in nonreproductive tissues, including three muscle clusters (muscles 5, 6, and 8) that appear to be largely restricted to female parasites (table S3), with muscle 8 representing muscle cells that surround the ovary (fig. S10). In some cases, we observed

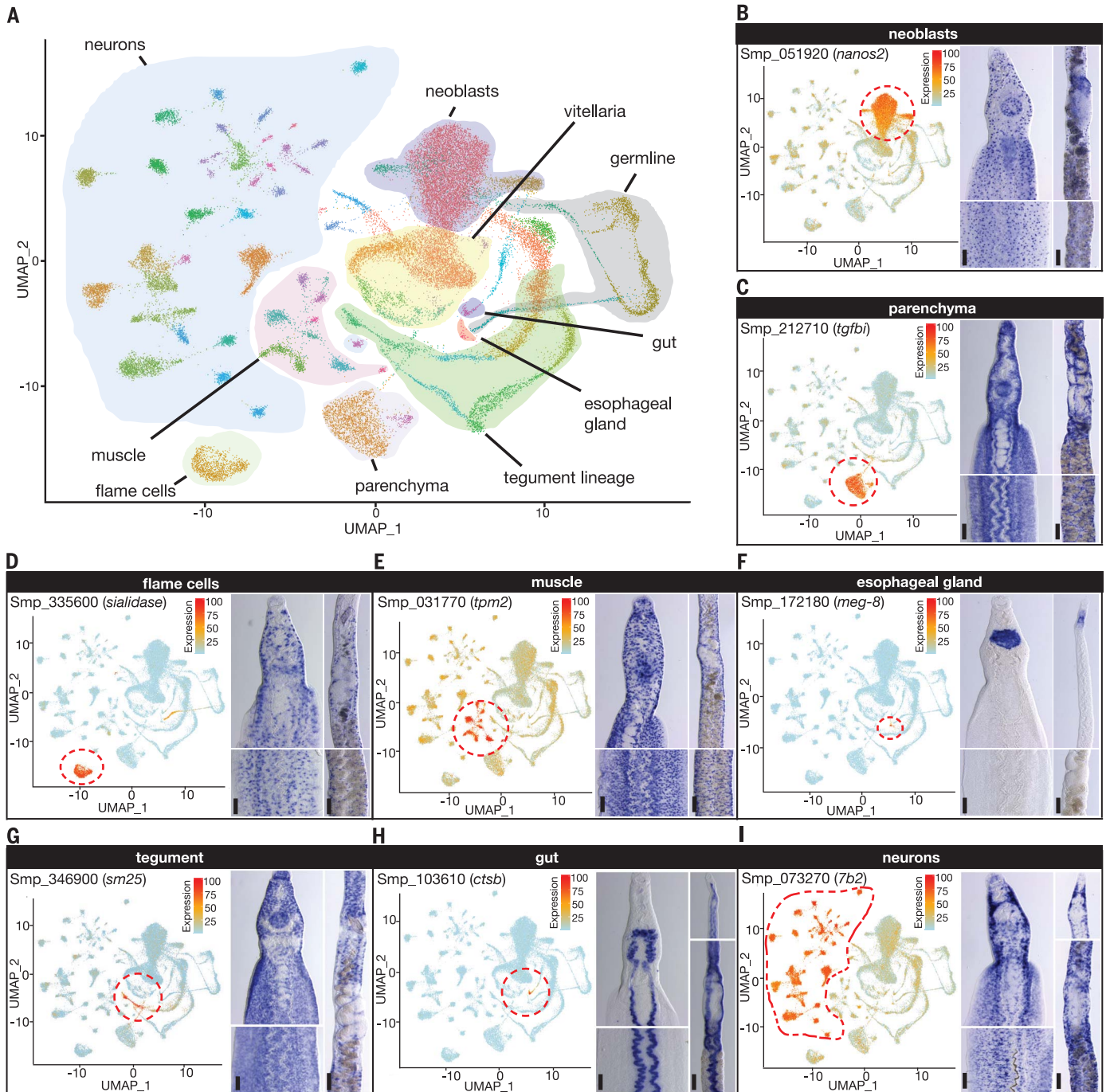


**Fig. 1. *S. mansoni* single-cell atlas.** (A) UMAP plot of the 68 scRNA-seq clusters. (B to I) UMAP plot (left) and whole-mount in situ hybridization (WISH) of the indicated gene and its expression in the noted tissue in the head (middle, top) and body (middle, bottom) of a male and the ovary (right, top) [(B) to (E) and (G)]

or the head (right, top) [(F), (H), and (I)] and vitellaria (right, bottom) of a mature female parasite. Scale bars are 100  $\mu$ m. UMAP plots are colored by gene expression (blue is low, and red is high). The regions enclosed by red dashed lines indicate the location of the relevant clusters on the UMAP plot.

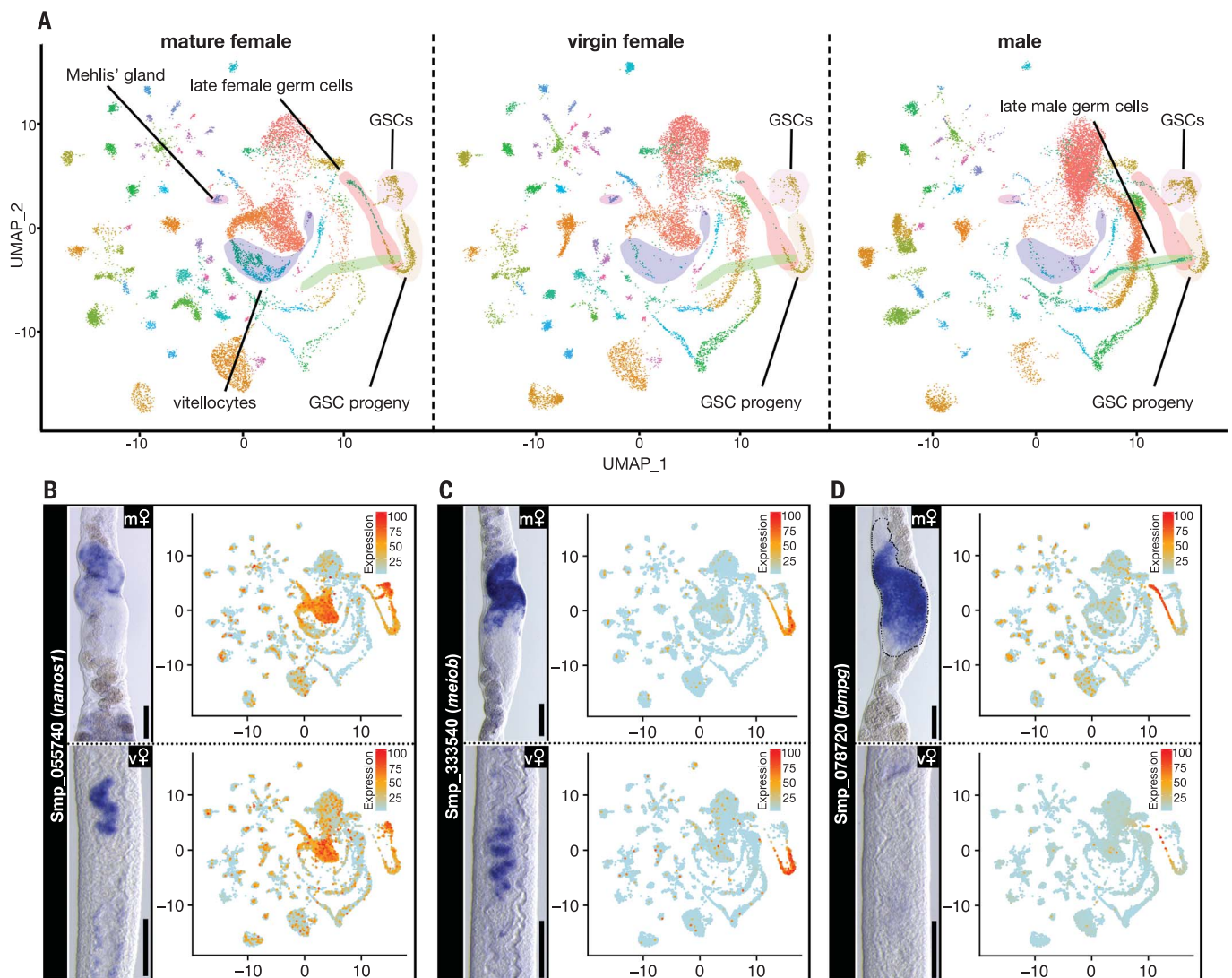


**Fig. 2. The germ lineage in schistosome ovaries.** (A) UMAP plots of all clusters split by parasite sex. Sexual tissues are labeled. (B to D) WISH (left) and UMAP plot (right) of gene expression of the indicated gene in sexually mature females (m♀) (top) and virgin females (v♀) (bottom) for the GSC marker *nanos1* (B), the GSC progeny marker *meioB* (C), and the late female germ cell marker *bmpg* (D). The dashed line in (D) indicates the boundary of the ovary. Scale bars are 100  $\mu$ m. UMAP plots are colored by gene expression (blue is low, and red is high).

unexpected numbers of male cells in clusters of female sexual tissues, which we attribute to neoblasts expressing low levels of differentiated tissue markers, similar to what has been observed in planarians (1) (fig. S11 and supplementary text).

Egg production is the primary driver of pathology, but this pathology is exacerbated by the parasite's stem cell-mediated longevity (3). Previous work suggests that adult neoblasts are molecularly homogeneous and predominantly give rise to cells involved in tegument production (4, 5), but free-living flatworms are known to possess functionally distinct neoblasts that produce specific tissues (18). We identified a subpopulation of neoblasts (*eled*<sup>+</sup> neoblasts) that formed a putative nontegument lineage as suggested by a linear "path" of cells from *eled*<sup>+</sup> neoblasts to the gut (Fig.

3A and fig. S12, A to F). These *eled*<sup>+</sup> neoblasts expressed *hnf4* (Fig. 3A and fig. S12, B and C), a marker of gut neoblasts in planarians (18). Given the importance of gut-mediated blood digestion for egg production (19), we sought to perturb this lineage by RNA interference (RNAi) of genes expressed in this lineage (fig. S13, A and B). We found that knocking down *hnf4* resulted in a ~3.8-fold increase in *eled*<sup>+</sup> neoblasts (Fig. 3B and fig. S13, C to F) and a concomitant decrease in the expression of several gut markers (fig. S14, A and B). Indeed, RNA-seq on *hnf4*(RNAi) animals demonstrated that more than 70% of transcripts expressed in the gut cluster were down-regulated (fig. S14, C and D; and table S4).

To understand whether stem cells functioned normally in *hnf4*(RNAi) animals, we first looked at apoptosis using terminal deoxy-

nucleotidyl transferase-mediated deoxyuridine triphosphate nick end labeling (TUNEL) and found no difference in *hnf4*(RNAi) animals, ruling out increased cell death (fig. S15A). Next, we looked at tegument production using 5-ethynyl-2'-deoxyuridine (EdU) pulse-chase approaches. We found a significant increase in tegument production in *hnf4*(RNAi) animals compared with controls (fig. S15, B and C), ruling out a broad stem cell-differentiation defect. Our ability to monitor new gut production by EdU pulse-chase approaches was complicated by the fact that gut marker expression was largely absent in most *hnf4*(RNAi) parasites (fig. S14, A and B). In cases where we could detect gut marker expression in EdU pulse-chase experiments, we found that gut-like tissue was being produced in *hnf4*(RNAi) parasites but was morphologically abnormal

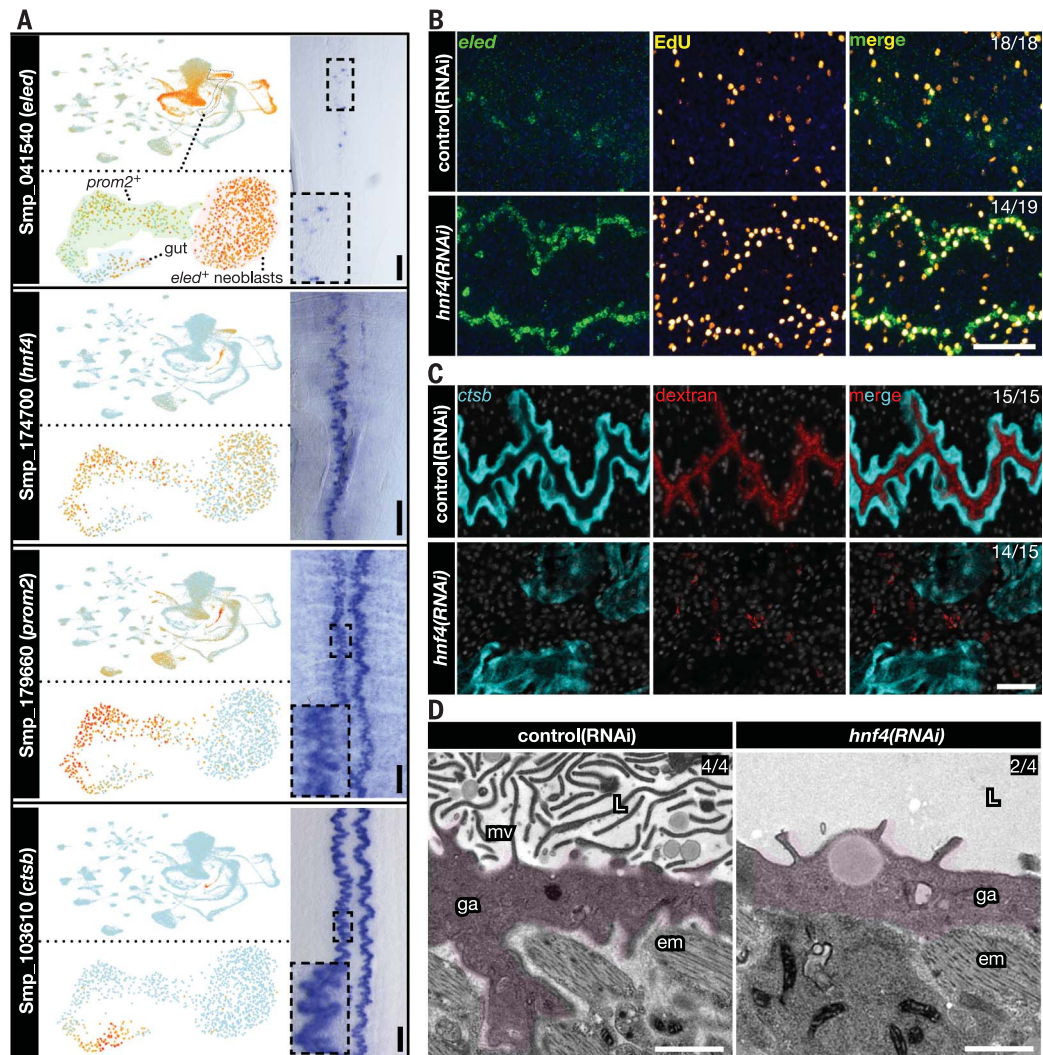


**Fig. 3. An *hnf4* homolog regulates a previously uncharacterized gut lineage.** (A) UMAP plots of the expression pattern of the indicated gene on the original dataset (left, top) or the reclustered dataset (left, bottom) and a colorimetric WISH (right) of a male parasite's trunk for *eled*, *hnf4*, *prom2*, and *ctsb*. The insets show magnifications of the regions enclosed by the dashed boxes. (B) FISH and EdU labeling showing the expression of *eled* (green) and EdU<sup>+</sup> proliferative cells (yellow) in control(RNAi) or *hnf4*(RNAi) animals.  $n \geq 18$  parasites, two biological replicates. (C) FISH of *ctsb* (cyan) and fluorescent

dextran (red) in the gut lumen in control(RNAi) and *hnf4*(RNAi) animals.  $n = 15$  parasites, three biological replicates. (D) TEM micrographs, showing the gut of control(RNAi) and *hnf4*(RNAi) animals. mv, microvilli; ga, gastrodermis; L, lumen; em, enteric muscle.  $n = 4$  parasites, two biological replicates. Nuclei are blue or gray in (B) and (C), respectively. The number of parasites similar to the representative image is in the upper-right corner of each panel. Scale bars are 100  $\mu\text{m}$  in (A), 50  $\mu\text{m}$  in (B), 20  $\mu\text{m}$  in (C), and 1  $\mu\text{m}$  in (D). UMAP plots are colored by gene expression (blue is low, and red is high).

(fig. S15D). Examination of the expression of *eled* and the gut marker *ctsb* revealed that locations where *eled*<sup>+</sup> neoblasts were abundant lacked normal gut tissue (fig. S15E). This suggests that the impairment of gut production is at least partially responsible for the gut defects after *hnf4* RNAi.

To assess gut structure, we next supplemented the culture media of *hnf4*(RNAi) parasites with fluorescently labeled dextran [which labels the gut lumen (20)]. After 12 hours of culture, all control(RNAi) parasites, but only 1 out of 15 *hnf4*(RNAi) parasites, had dextran in the lumen (Fig. 3C). The dextran failed to enter the digestive tract of the *hnf4*(RNAi) parasites (fig. S16A), suggesting either a com-

plete loss of patency or a defect in the parasite's ability to coordinate dextran ingestion. We then examined *hnf4*(RNAi) animals by transmission electron microscopy (TEM). The schistosome gut is a syncytial blind tube-like structure with a microvilli-filled lumen (21). Though gut tissue was still present, we found a significant decrease in luminal microvilli (Fig. 3D and fig. S16B) and two out of four *hnf4*(RNAi) animals had dilated lumens compared with controls (fig. S16C).

To assess the digestive capability of *hnf4*(RNAi) parasites, we added red blood cells (RBCs) to the media and observed the parasites' ability to uptake and digest the cells. *hnf4*(RNAi) parasites failed to either ingest (15/69) or digest

RBCs (54/69) (Fig. 4A and fig. S17A). Because we observed a decrease in the expression of proteolytic enzymes by RNA-seq (table S4), we studied whether *hnf4* RNAi resulted in loss of cysteine (cathepsin) protease activity [which contributes to hemoglobin digestion (22, 23)]. By measuring cathepsin activity of lysates in *hnf4*(RNAi) parasites using a fluorogenic peptidyl substrate, we found that cathepsin B activity was decreased 8.2-fold relative to that in control parasites (Fig. 4B), consistent with gene expression analyses (table S4). By contrast, aspartyl protease activity was similar in control and *hnf4*(RNAi) parasites (fig. S17B), which could reflect expression of aspartic proteases in nongut tissues that were unaffected after

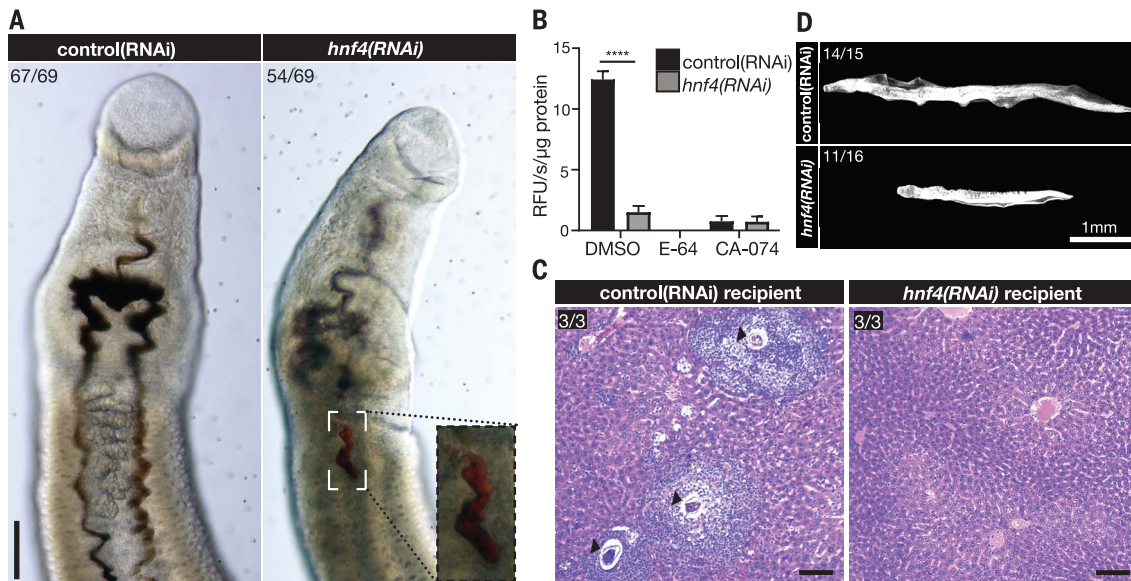


**Fig. 4. *hnf4* is required for blood feeding and pathology.** (A) Brightfield microscopy images of control(RNAi) or *hnf4*(RNAi) animals cultured with RBCs. The inset shows a magnification of the boxed area. (B) Cathepsin activity of lysates from control(RNAi) or *hnf4*(RNAi) animals, as determined by cleavage of Z-FR-AMC peptide substrate with no inhibitor [dimethyl sulfoxide (DMSO)], a broad cysteine protease inhibitor (E-64), or a cathepsin B-selective inhibitor (CA-074).  $n = 3$  biological replicates of assays carried out in technical triplicates. Error bars indicate

95% confidence interval. \*\*\*\* $p < 0.0001$  (Welch's  $t$  test). RFU, relative fluorescence units. (C) Hematoxylin and eosin (H&E)-stained mouse liver sections 22 days after transplant with RNAi-treated parasites. Arrowheads show granulomata. Sections are from  $n = 3$  recipients. (D) Parasites recovered from transplant recipients.  $n > 15$  parasites from three recipients. Nuclei are white. The number of parasites or sections similar to the representative micrograph is in the upper-left corner of each panel. Scale bars are 100  $\mu\text{m}$  in (A) and (C) and 1 mm in (D).

*hnf4* RNAi (tables S1 and S4). Together, these data suggest that *hnf4* is at least indirectly required for the digestion of hemoglobin, in part by regulating the expression of cathepsin B, which is a key contributor to the digestion of blood proteins, including hemoglobin (22, 23), in *S. mansoni*.

We examined whether *hnf4* was required to cause disease in the host by transplanting control and *hnf4*(RNAi) parasites into uninfected mice and then perfusing the mice 22 to 30 days after transplant. Worm recovery was statistically indistinguishable [control(RNAi) = 72% versus *hnf4*(RNAi) = 49%,  $p = 0.136$ , Welch's  $t$  test] (fig. S17C). This observation is not entirely unexpected because schistosomes can acquire nutrients through their tegument (19). Nonetheless, mice receiving *hnf4*(RNAi) parasites had morphologically normal livers in contrast to abundant egg-induced granulomata in livers of control parasite recipients (Fig. 4C and fig. S17D). Additionally, recovered male *hnf4*(RNAi) parasites were significantly shorter than controls (2.87 versus 5.21 mm, respectively;  $p < 0.0001$ ; Welch's  $t$  test) (Fig. 4D and fig. S17E). These results show that *hnf4* is at least indirectly required for parasite growth and egg-induced pathology in vivo. Together, these data suggest that *hnf4*, specifically, and gut homeostasis, generally, are potential therapeutic targets to blunt the pathology caused by adult parasites.

Here, we describe a comprehensive single-cell atlas of the adult schistosome, identify

regulators of gut biology, and leverage this knowledge to experimentally block schistosome-induced pathology in the host. We envision these data serving as a catalyst toward understanding other aspects of schistosome biology (e.g., reproductive biology) and serving as a foundation for understanding the development of various cellular lineages during the parasite life cycle. Indeed, our approach serves as a template for the investigation of other understudied and experimentally challenging parasitic metazoans, improving our understanding of their biology and enabling the discovery of therapies for these pathogens.

#### REFERENCES AND NOTES

- C. T. Fincher, O. Wurtzel, T. de Hoog, K. M. Kravarik, P. W. Reddien, *Science* **360**, eaaq1736 (2018).
- B. Wang *et al.*, *eLife* **7**, e35449 (2018).
- J. J. Collins III *et al.*, *Nature* **494**, 476–479 (2013).
- G. R. Wendt *et al.*, *eLife* **7**, e33221 (2018).
- J. J. Collins III, G. R. Wendt, H. Iyer, P. A. Newmark, *eLife* **5**, e12473 (2016).
- J. Wang, J. J. Collins III, *Int. J. Parasitol.* **46**, 405–410 (2016).
- G. P. Dillon, J. C. Illes, H. V. Isaacs, R. A. Wilson, *Parasitology* **134**, 1589–1597 (2007).
- Z. Lu *et al.*, *Sci. Rep.* **6**, 31150 (2016).
- P. F. Basch, *Schistosomes: Development, Reproduction, and Host Relations* (Oxford Univ. Press, 1991).
- R. A. Wilson, L. A. Webster, *Biol. Rev. Camb. Philos. Soc.* **49**, 127–160 (1974).
- L. E. Cote, E. Simental, P. W. Reddien, *Nat. Commun.* **10**, 1592 (2019).
- J. N. Witchley, M. Mayer, D. E. Wagner, J. H. Owen, P. W. Reddien, *Cell Rep.* **4**, 633–641 (2013).
- I. Popiel, D. L. Irving, P. F. Basch, *Tissue Cell* **17**, 69–77 (1985).
- E. J. Pearce, A. S. MacDonald, *Nat. Rev. Immunol.* **2**, 499–511 (2002).

- P. M. Nollen, R. D. Floyd, R. G. Kolzow, D. L. Deters, *J. Parasitol.* **62**, 227–231 (1976).
- S. E. Galanti, S. C. Huang, E. J. Pearce, *PLOS Negl. Trop. Dis.* **6**, e1509 (2012).
- M. K. Shaw, D. A. Erasmus, *J. Helminthol.* **56**, 51–54 (1982).
- J. C. van Wolfswinkel, D. E. Wagner, P. W. Reddien, *Cell Stem Cell* **15**, 326–339 (2014).
- P. J. Skelly, A. A. Da'dara, X. H. Li, W. Castro-Borges, R. A. Wilson, *PLOS Pathog.* **10**, e1004246 (2014).
- S. L. Hall *et al.*, *Mol. Biochem. Parasitol.* **179**, 18–29 (2011).
- G. P. Morris, *Experientia* **24**, 480–482 (1968).
- C. R. Caffrey, L. Goupil, K. M. Rebello, J. P. Dalton, D. Smith, *PLOS Negl. Trop. Dis.* **12**, e0005840 (2018).
- M. Sajid *et al.*, *Mol. Biochem. Parasitol.* **131**, 65–75 (2003).
- J. Collins, A single-cell RNAseq atlas of *Schistosoma mansoni* identifies a key regulator of blood feeding, v2, dataset. Dryad (2020); <https://doi.org/10.5061/dryad.0k6djt9xk>.

#### ACKNOWLEDGMENTS

We thank C. Paz for technical assistance and G. Hon for expertise in scRNA-seq library preparation. Schistosome-infected mice and *Biophalaria glabrata* snails were provided by the National Institute of Allergy and Infectious Diseases (NIAID) Schistosomiasis Resource Center of the Biomedical Research Institute (Rockville, MD, USA) through National Institutes of Health (NIH)-NIAID contract HHSN2722017000141 for distribution through BEI Resources. FACS was performed with the aid of the Moody Foundation Flow Cytometry Facility at the University of Texas Southwestern Medical Center (UTSW). TEM imaging and sample preparation was performed with the aid of the Electron Microscopy Core at UTSW. RNA-seq was performed with the aid of the McDermott Center Next Generations Sequencing Core at UTSW. **Funding:** This work was supported by NIH grants R01R01A121037 (J.J.C.), R01R01A1150715 (M.L.R.), R21R21A1133393 (A.J.O.D.), and F30F30A1131509-01A1 (G.W.); Welch Foundation grants I-1948-20180324 (J.J.C.) and I-1936-20170325 (M.L.R.); National Science Foundation grant MCB1553334 (M.L.R.); the Burroughs Wellcome Fund (J.J.C.); Wellcome Trust grant 107475/Z/15/Z (J.J.C.); and Bill and Melinda Gates Foundation grant OPP1171488 (C.R.C.). **Author contributions:** Conceptualization: G.W., L.Z., R.C., C.L., A.J.O.D., C.R.C., J.J.C.; Investigation: G.W., L.Z., R.C., C.L., J.J.C.; Designing web-based resources: M.L.R.; Writing – original draft: G.W., L.Z., J.J.C.; Writing – review and editing: all authors. **Competing interests:** The authors declare no competing interests.

**Data and materials availability:** A searchable database of scRNA-seq data can be accessed at [www.collinslab.org/schistocyte](http://www.collinslab.org/schistocyte); raw scRNA-seq plots can be accessed at Dryad (24). Raw and some processed data from scRNA-seq and *hnf4* RNAi RNA-seq experiments have been deposited in the NCBI Gene Expression Omnibus under accession number GSE146737.

**SUPPLEMENTARY MATERIALS**

[science.sciencemag.org/content/369/6511/1644/suppl/DC1](http://science.sciencemag.org/content/369/6511/1644/suppl/DC1)  
Materials and Methods  
Supplementary Text  
Figs. S1 to S18  
Tables S1 to S7

References (25–34)  
MDAR Reproducibility Checklist

[View/request a protocol for this paper from Bio-protocol.](#)

17 March 2020; accepted 31 July 2020  
10.1126/science.abb7709

## A single-cell RNA-seq atlas of *Schistosoma mansoni* identifies a key regulator of blood feeding

George Wendt, Lu Zhao, Rui Chen, Chenxi Liu, Anthony J. O'Donoghue, Conor R. Caffrey, Michael L. Reese and James J. Collins III

*Science* **369** (6511), 1644-1649.  
DOI: 10.1126/science.abb7709

### Schistosome biology illuminated

Schistosomiasis is caused by a parasitic flatworm about which little is known. Therefore, options to combat human disease caused by schistosome infection are limited. To aid in our quest to develop treatments, two studies undertook molecular investigations of the parasite *Schistosoma mansoni*. By generating a single-cell atlas, Wendt *et al.* identified the developmental trajectory of the flatworm, including the blood-feeding gut required for its survival in the host. From these data, they found a gene required for gut development that, when knocked out through RNA interference, confers reduced pathology in infected mice. Wang *et al.* performed a large-scale RNA interference survey of *S. mansoni* and identified an essential pair of protein kinases that can be targeted by approved pharmacological intervention (see the Perspective by Anderson and Duraisingh). These molecular investigations add to our understanding of the schistosome parasite and provide biological information that may help to combat this neglected tropical disease.

*Science*, this issue p. 1644, p. 1649; see also p. 1562

#### ARTICLE TOOLS

<http://science.sciencemag.org/content/369/6511/1644>

#### SUPPLEMENTARY MATERIALS

<http://science.sciencemag.org/content/suppl/2020/09/23/369.6511.1644.DC1>

#### RELATED CONTENT

<http://science.sciencemag.org/content/sci/369/6511/1562.full>  
<http://science.sciencemag.org/content/sci/369/6511/1649.full>  
<http://stm.sciencemag.org/content/scitransmed/12/529/eaaw9522.full>  
<http://stm.sciencemag.org/content/scitransmed/12/558/eabc0441.full>  
<http://stm.sciencemag.org/content/scitransmed/12/540/eaay0605.full>  
<http://stm.sciencemag.org/content/scitransmed/12/524/eaaw3703.full>

#### REFERENCES

This article cites 32 articles, 1 of which you can access for free  
<http://science.sciencemag.org/content/369/6511/1644#BIBL>

#### PERMISSIONS

<http://www.sciencemag.org/help/reprints-and-permissions>

Use of this article is subject to the [Terms of Service](#)

---

*Science* (print ISSN 0036-8075; online ISSN 1095-9203) is published by the American Association for the Advancement of Science, 1200 New York Avenue NW, Washington, DC 20005. The title *Science* is a registered trademark of AAAS.

Copyright © 2020 The Authors, some rights reserved; exclusive licensee American Association for the Advancement of Science. No claim to original U.S. Government Works